Atmospheric Internal Variability in the Summer Indo–Northwestern Pacific: Role of the Intraseasonal Oscillation

XUDONG WANG

Collaborative Innovation Center on Forecast and Evaluation of Meteorological Disaster/KLME/ILCEC, Nanjing University of Information Science and Technology, Nanjing, China, and Scripps Institution of Oceanography, University of California, San Diego, La Jolla, California

SHANG-PING XIE

Scripps Institution of Oceanography, University of California, San Diego, La Jolla, California

ZHAOYONG GUAN

Collaborative Innovation Center on Forecast and Evaluation of Meteorological Disaster/KLME/ILCEC, Nanjing University of Information Science and Technology, Nanjing, China

(Manuscript received 22 October 2019, in final form 6 January 2020)

ABSTRACT

Summer atmospheric interannual variability in the Indo-northwestern Pacific (NWP) is coupled with tropical sea surface temperature (SST) variability. This study investigates the importance and origin of atmospheric internal variability in the Indo-NWP region. Using the reanalysis and the 30-member atmospheric model simulation, two SST-related interannual modes are identified in the Indo-NWP region during boreal summer with the month-reliant empirical orthogonal function analysis. The first mode is related to concurrent El Niño-Southern Oscillation originating from the eastern equatorial Pacific whereas the second mode features an anomalous anticyclone (AAC) in post–El Niño summers over the NWP region, known as the Indo-western Pacific Ocean capacitor. The SST-induced modes show temporal persistence from June to August. The residual variability is the focus of this study. The dominant mode of the residual variability displays an AAC structure over the NWP but little month-to-month persistence, indicative of atmospheric internal dynamics unrelated to SST forcing. Further investigation suggests the monthly internal AAC arises from the summer intraseasonal oscillation (ISO). The broad band of ISO yields nonzero monthly means that project strongly onto the AAC pattern. Finally, the anomalies of rainfall and low-level circulation in summer 2016 are investigated. The reversal of the low-level circulation pattern from an AAC in July to an anomalous cyclone over the NWP in August 2016 is due to the ISO-induced internal variability.

1. Introduction

Summer climate over the Indo-northwestern Pacific (NWP) is strongly affected by El Niño-Southern Oscillation (ENSO). Following the major El Niño event in winter 1997/98, atmospheric convection and tropical cyclone activity were both suppressed over the tropical NWP region in summer 1998, consistent with the Indowestern Pacific Ocean capacitor (IPOC) effect (Xie et al. 2016). In May to July of 2016, rainfall and tropical cyclone count were below normal over the NWP, similar to the circumstances in 1998 (Li et al. 2017; Takaya et al. 2017).

Corresponding author: Xudong Wang, xdwang_1992@163.com

In August 2016, however, convection and tropical cyclone activity unexpectedly increased over the NWP (Huangfu et al. 2018; Chowdary et al. 2019). This study is motivated by the wish to understand the deviations of NWP climate anomalies from the post–El Niño IPOC effect.

In the tropics, sea surface temperature (SST) variability is an important driver for variability in rainfall and atmospheric circulations, both locally and remotely (Deser et al. 2010). ENSO is the dominant mode of interannual variability with global influence (Alexander et al. 2002; Trenberth et al. 2002). ENSO develops in boreal summer, peaks in winter, and decays rapidly in the following spring. ENSO influence on the Indo-NWP spans two summers, concurrent and subsequent. During

El Niño developing summer, the tropical convection center shifts eastward from the Maritime Continent to the central-western Pacific, weakening the Walker circulation. The weakened Walker circulation in the Indian Ocean causes Indian monsoon rainfall to decrease (Rasmusson and Carpenter 1983; Webster and Yang 1992; Mishra et al. 2012). Suppressed convection over the northwestern Pacific during El Niño further affects East Asia climate through the westward extension of the anomalous subtropical high (Zhang et al. 1999). During post-El Niño summer, El Niño itself has dissipated in the equatorial eastern Pacific, but its climatic impact lingers over the tropical Indo-northwest Pacific region, affecting the Indian summer monsoon (ISM) onset, rainfall, and surface air temperature over India (Mishra et al. 2012; Zhou et al. 2019). The ENSO-induced tropical Indian Ocean warming excites the warm tropospheric Kelvin wave propagating into the western Pacific. The associated Ekman divergence in the NWP suppresses convection and triggers an anomalous anticyclone (AAC) in the NWP (Xie et al. 2009). The SST cooling in the NWP also helps maintain the AAC through the atmospheric Rossby wave response (Wang et al. 2003; Wu et al. 2010). The El Niño-related AAC over the NWP further affects East Asia through the meridional Rossby wave train, the so-called Pacific-Japan teleconnections (PJ; Nitta 1987; Kosaka et al. 2013; Xu et al. 2019).

The instraseasonal oscillation (ISO), especially the Madden-Julian oscillation (MJO), is planetary-scale waves with periods of 30-60 days propagating eastward along the equator (Madden and Julian 1971, 1972; Zhang 2005). The tropical ISO exhibits remarkable seasonal variations (Wang and Rui 1990; Adames et al. 2016; Jiang et al. 2018). In boreal summer, the ISO shows complex propagating features. Prominent northward and northeastward propagations of the summer ISO were found over the Asian monsoon region (Yasunari 1980; Annamalai and Slingo 2001). The summer monsoon ISO (MISO) in the Indian Ocean propagates from the south of the equator to the Indian peninsula and foothills of the Himalayas, affecting the monsoon onset (Murakami et al. 1986; Joseph et al. 1994) and active/break cycles of the monsoon (Webster et al. 1998; Annamalai and Slingo 2001; Zhou et al. 2019). The northeastward propagation of ISO also causes the flooding and heat waves over the East Asian monsoon region (Mao and Wu 2006; Hsu et al. 2017).

Low seasonal predictability of India summer rainfall indicates the existence of significant internal variability over the Asian monsoon region (Goswami 1998). Several studies suggested connections between MISO and seasonal mean interannual variability over the Indian

Ocean. Goswami and Mohan (2001) showed that the intraseasonal and interannual variability of the ISM shares a common spatial pattern. Goswami and Xavier (2005) further indicated that MISO is responsible for internal interannual variability of the ISM. To the extent that MISO is not modulated by SST variations, they argued the internal interannual variability of ISM is decoupled from SST forcing. Sperber et al. (2000) suggested that strong monsoons are associated with higher probability of occurrence of active phases of ISO.

The present study examines the interannual variability from June to August in the Indo-NWP region and the relationship to atmospheric internal variability, the summer ISO in particular. We wish to address the following questions: How much of the observed variance can be explained by the internal variability over the Indo-NWP? How does the leading internal mode look? Is it distinct from the SST-forced modes? How much does the summer ISO contribute to the internal variability? Previous studies mainly focused on the MISO and its relationship with the ISM variability over the Indian Ocean (Goswami and Mohan 2001; Goswami and Xavier 2005) but they paid little attention to the ISO-interannual variability relationship in the NWP region, where the intraseasonal to interannual variability is comparable in magnitude to that in the Indian Ocean (Goswami 2012). Our analysis for 1979–2017 shows that the internal variability indeed arises from the summer ISO, but the leading mode is distinct from the ISM mode in spatial structure, with large loading in the NWP. We return to discuss the unusual climate state in August 2016 over the Indo-NWP and evaluate the contributions of the summer ISO.

The rest of the paper is organized as follows. Section 2 describes the data and methods. Section 3 briefly shows the rainfall and circulation anomalies in summer 2016. Section 4 examines the SST-related and internal variability over the Indo-NWP. Section 5 discusses relationship between the internal variability and the summer ISO. Section 6 analyzes the ISO contributions for the unusual climate state in August 2016. Section 7 summarizes and discusses our results.

2. Datasets and methods

a. Observations

We use the daily European Centre for Medium-Range Weather Forecasts interim reanalysis (ERA-Interim; Dee et al. 2011) winds and precipitation with a horizontal resolution of $1.5^{\circ} \times 1.5^{\circ}$. The monthly SST dataset is from the Met Office Hadley Centre (Rayner et al. 2003), with $1^{\circ} \times 1^{\circ}$ resolution.

The present study focuses on intraseasonal and interannual variability. For the interannual variability, the monthly anomalies are derived relative to the climatological mean over the whole period (1979–2017) after removing the linear trend and the decadal variability (longer than 10 years) by using the Lanczos high-pass filter. For the intraseasonal variability, we use the 20–100-day Lanczos bandpass filter (Duchon 1979).

b. AMIP simulation

To examine the atmospheric variability associated with the global SST forcing, we utilize a 30-member ensemble of ECHAM5 atmospheric model simulations [available online at the Facility for Climate Assessments (FACTS) website; see https://www.esrl.noaa.gov/psd/ repository/alias/facts]. The ECHAM5 model was run at spectral T159 ($\sim 0.75^{\circ} \times \sim 0.75^{\circ}$) horizontal resolution with 17 vertical levels. The model is forced with historical global SSTs based on Hurrell et al. (2008), which are a merged product of the monthly mean Hadley Centre Sea Ice and SST dataset version 1 (HadISST1; Rayner et al. 2003) and version 2 of the NOAA weekly optimum interpolation (OI) SST analysis (Reynolds et al. 2002). A complete description of the model can be found in Roeckner et al. (2003). Each ECHAM5 run covers the period of 1979– 2017, starting with different initial conditions.

We use the raw output to compute the ensemble mean, and the ensemble spread of the ECHAM5 AMIP runs. As the 30 members share the same external forcing, the ensemble mean represents the prescribed SST-forced variability. Obtained by subtracting the ensemble mean from the raw output, the ensemble spread captures atmospheric internal variability as different initial conditions of each member run randomize the phasing of atmospheric internal variability.

c. Methodology

We perform month-reliant EOF analysis of normalized 850- and 200-hPa zonal and meridional wind anomalies in the Indo-western Pacific (10°S–25°N, 40°–140°E) during June to August to extract leading modes of the monthly variability. Unlike the conventional EOF for a single month or season, the month-reliant EOF investigates the wind anomalies in a sequence from June to August. Each eigenvector represents a set of three sequential monthly spatial patterns that share the same yearly principal component (PC).

For the summer ISO, we conduct an EOF analysis of daily normalized upper and lower troposphere wind anomalies in the Indo-NWP from June to August over the period of 1979–2017. We compared with the boreal summer intraseasonal oscillation (BSISO) indices of Lee et al. (2013), derived from the first two leading

multivariate EOFs of outgoing longwave radiation (OLR) and 850-hPa zonal wind anomalies in the Asian monsoon region. Our EOF modes are almost identical to the BSISO modes and capture a more robust northward propagation than Real-time Multivariate MJO (RMM) indices (Wheeler and Hendon 2004).

3. Climate anomalies in summer 2016

We start by comparing the monthly evolution of rainfall and lower tropospheric wind anomalies from June to August during summer 2016 between observations and the ECHAM5 AMIP ensemble mean. In the tropical northwestern Pacific (Figs. 1a,b), a weak anticyclone is observed, accompanied with decreased rainfall from June to July. Meanwhile, a cyclonic circulation accompanied by enhanced precipitation is found east of Japan. In general, during post-El Niño summer, the AAC appears over the Indo-western Pacific in response to the concurrent Indian Ocean warming, along with a cyclonic circulation to the north as a part of the Pacific–Japan teleconnection pattern (Nitta 1987; Kosaka and Nakamura 2010; Kosaka et al. 2013; Xie et al. 2016). Summer 2016 follows a major El Niño event of 2015/16, but the weak anticyclone disappears in August replaced with a cyclonic circulation and increased rainfall over the NWP region (Fig. 1c). This peculiar reversal of circulation and rainfall patterns from July to August cannot be explained by the IPOC effect that persists through summer. To evaluate the SST effect, we analyze the precipitation and 850-hPa wind anomalies in the ECHAM5 AMIP ensemble mean (Figs. 1d-f). A weak IPOC mode is found in the NWP but southward shifted slightly as compared to the observations from June to July (Figs. 1d,e). Unlike observations, the model ensemble mean displays a sustained AAC over the NWP in August (Fig. 1f). The discrepancies of rainfall and lowlevel wind anomalies in August between observations and the model ensemble mean suggests that SST forcing has limited impact on the establishment of the anomalous cyclone in the NWP. Indeed, previous results found that the positive SST anomalies over the Indo-NWP persists from June to August in 2016 (Huangfu et al. 2018; Chowdary et al. 2019; Chen et al. 2019). Since the atmospheric variability in AMIP ensemble mean is mainly driven by the prescribed SSTs, the inconsistency between observations and the model ensemble mean is due to atmospheric internal variability.

4. Separating the SST effect and internal variability

a. SST-induced variability

To obtain the SST-forced variability, we first conduct a month-reliant EOF analysis of normalized upper and

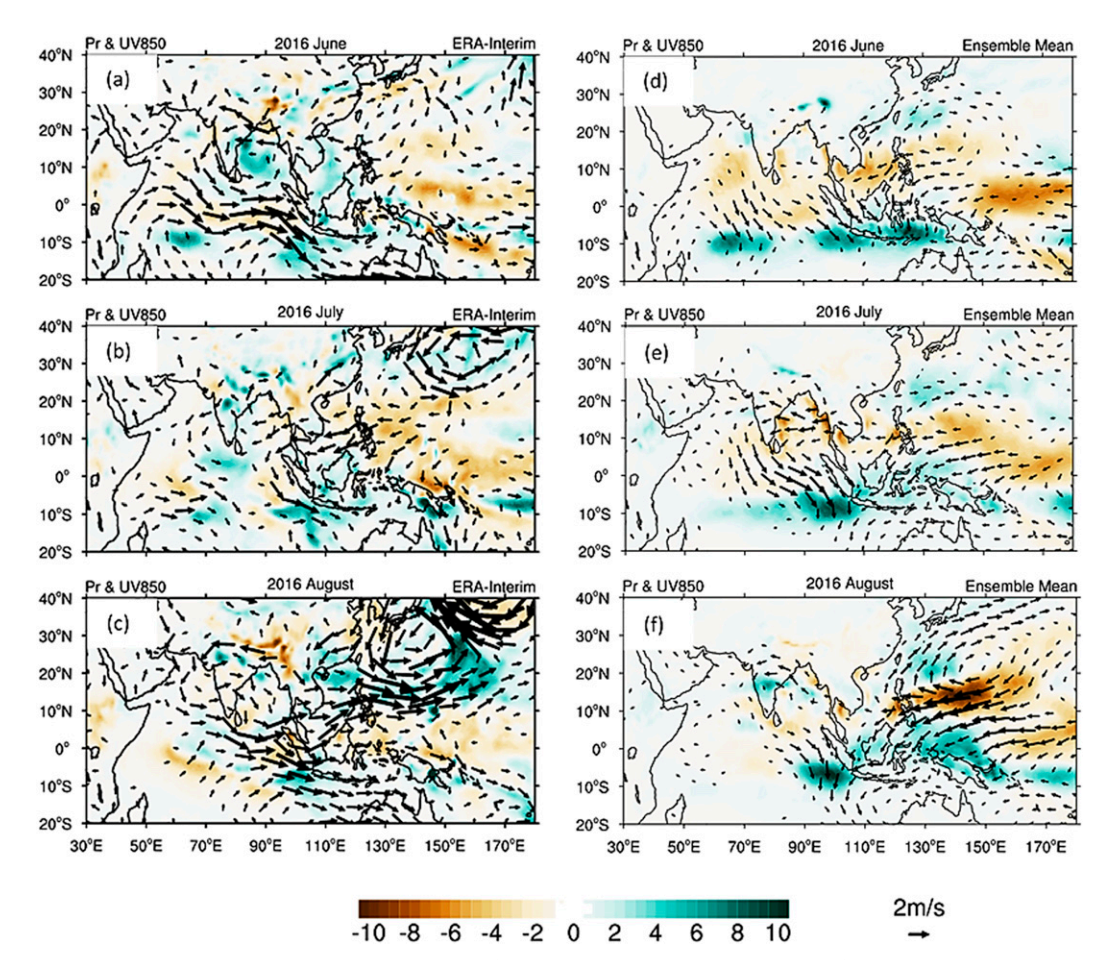


FIG. 1. Monthly mean rainfall (shading; mm day⁻¹) and lower-level wind (vectors; m s⁻¹) anomalies from June to August in 2016: (a)–(c) observations and (d)–(f) ECHAM5 AMIP ensemble mean.

lower tropospheric wind anomalies from June to August for 1979–2017 in both observations and model ensemble mean. Figures 2a-f show monthly anomalies of rainfall and 850-hPa winds from June to August regressed onto the first principal component (PC_1^{SST}) of month-reliant EOF. The first EOF mode (EOF₁^{SST}) of observations explains 13.8% of the total wind variance and is related to concurrent developing El Niño events (Figs. 2a-c). The correlation between the first mode and concurrent summer Niño-3.4 index amounts to 0.86. During El Niño summers, the westerly wind anomalies prevail in the tropical western Pacific, increasing rainfall in the equatorial western Pacific and decreasing precipitation over the Maritime Continent and Indian peninsula (Webster and Yang 1992). The anomalous westerly winds advance eastward gradually from June to August, coupled with the eastward shifting of convection center. The first EOF mode of the ensemble mean captures 24.2% of the total wind variance and resembles the observations (Figs. 2d-f). Correlation between the ensemble mean

PC₁^{SST} and concurrent Niño-3.4 index is 0.83. The PC₁^{SST} correlation between observations and the model ensemble mean amounts to 0.76 (Fig. 4a), suggesting that the AMIP ensemble mean shows skill in simulating the SST-forced variability. Two strong El Niño events (1997 and 2015) are well captured in observations and the model ensemble mean.

The second month-reliant EOF mode (EOF₂^{SST}) of observations (Figs. 3a–c) captures 12.3% of the total wind variance and is well separated from the first and third modes by the criterion of North et al. (1982). The second mode is the IPOC, which often occurs during post–El Niño summers (Xie et al. 2016). Indeed, the correlation of the second PC (PC₂^{SST}) with preceding DJF Niño-3.4 index and concurrent JJA north Indian Ocean (NIO) SST index (0°–20°N, 40°–110°E) amounts to 0.58 and 0.71, respectively. Prominent features during post–El Niño summer include a warming tropical Indian Ocean and South China Sea and an AAC over the NWP region, resulting from positive feedback of the regional ocean—

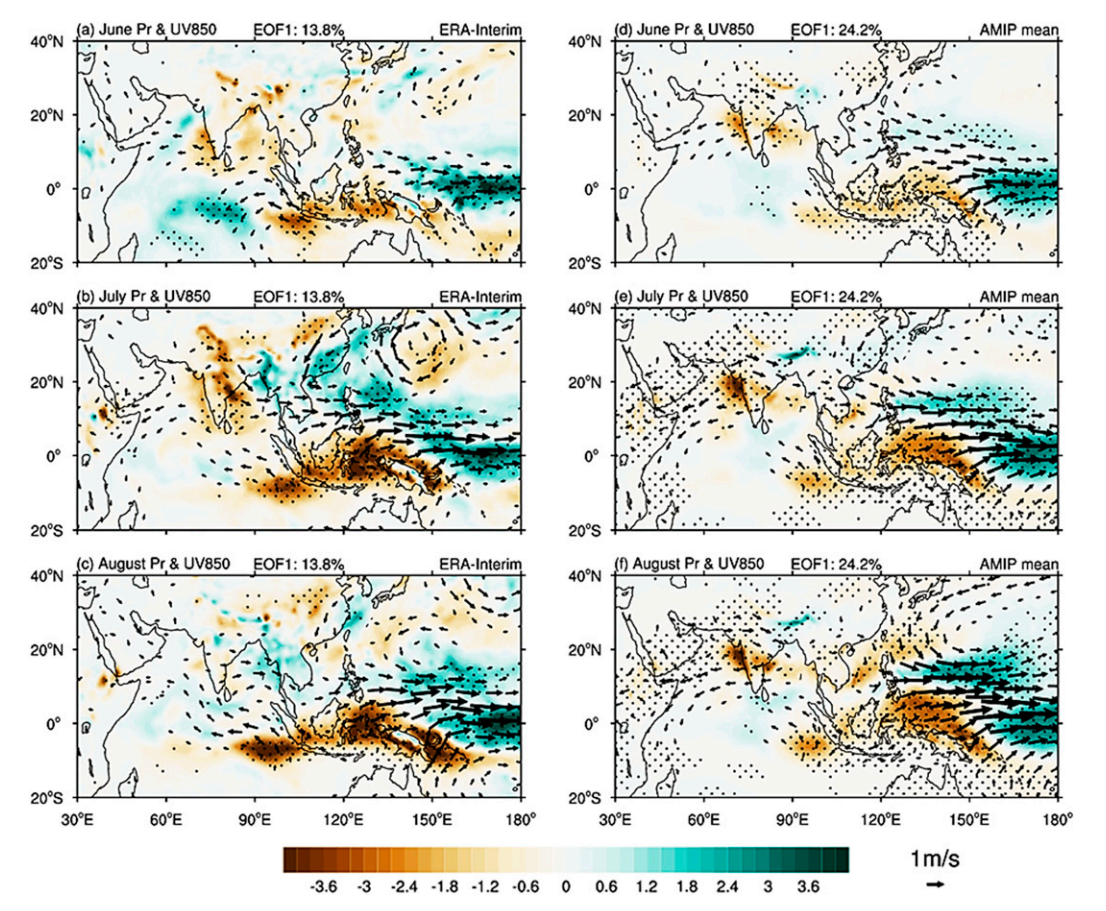


FIG. 2. The rainfall (shading; mm day⁻¹) and lower-level winds (vectors; m s⁻¹) regressed against the first monthreliant EOF PC₁^{SST}: (a)–(c) observations and (d)–(f) ECHAM5 AMIP ensemble mean. Stippling represents the rainfall anomalies >99% confidence level, based on the t test.

atmosphere coupling that prolongs the El Niño influence (Du et al. 2009; Kosaka et al. 2013; Zhou et al. 2018). The NIO warming is associated with the anomalous easterly winds on the south flank of the NWP AAC, which reduce the monsoon southwesterlies and surface evaporation. The NIO warming, on the other hand anchors the NWP AAC via the Kelvin wave-convection adjustment (Xie et al. 2009, 2016). The IPOC mode is captured in the model ensemble mean (Figs. 3d-f) and explains 20.4% of total wind variance. Correlations of PC₂^{SST} in the model ensemble mean with antecedent DJF Niño-3.4 index and concurrent NIO index are 0.46 and 0.68, respectively. The imperfect correlation with antecedent ENSO indicates coupled IPOC variability unrelated to ENSO (Wang et al. 2020). The correlation of PC₂^{SST} between observations and the model ensemble mean is 0.58 (Fig. 4b). The persistence of the IPOC pattern from June to August in EOF₂^{SST} suggests that slow evolving SST forcing over the Indo-Pacific basin induces a prolonged atmospheric pattern in post-ENSO summer. In 2016, PC₂^{SST} of the ensemble mean indicates a weak IPOC mode while the observed anomalies are nearly at a neutral state (Fig. 4b).

The third month-reliant EOF (EOF $_3^{SST}$) in observations (Figs. 5a-c) shows little month-to-month persistence in spatial pattern: an intensified ISM with southwesterly wind anomalies in the lower troposphere and weakened East Asian summer monsoon with an anomalous anticyclone over the coastal region of China in June. Then the rainfall pattern and low-level circulation change suddenly in July and turn into an anomalous cyclone over the NWP in August with westerly wind and increased rainfall anomalies in its south flank. However, the AMIP ensemble mean (Figs. 5d-f) exhibits enhanced rainfall anomalies and relatively weak winds in the north Indian Ocean from June to August. The PC₃^{SST} correlation between observations and the model ensemble mean is only 0.07. Since atmospheric variability in the model ensemble mean is mainly driven by the SST forcing, the low correlation of PC₃^{SST} and inconsistency of the EOF₃SST spatial pattern between observation and the model ensemble mean indicate that

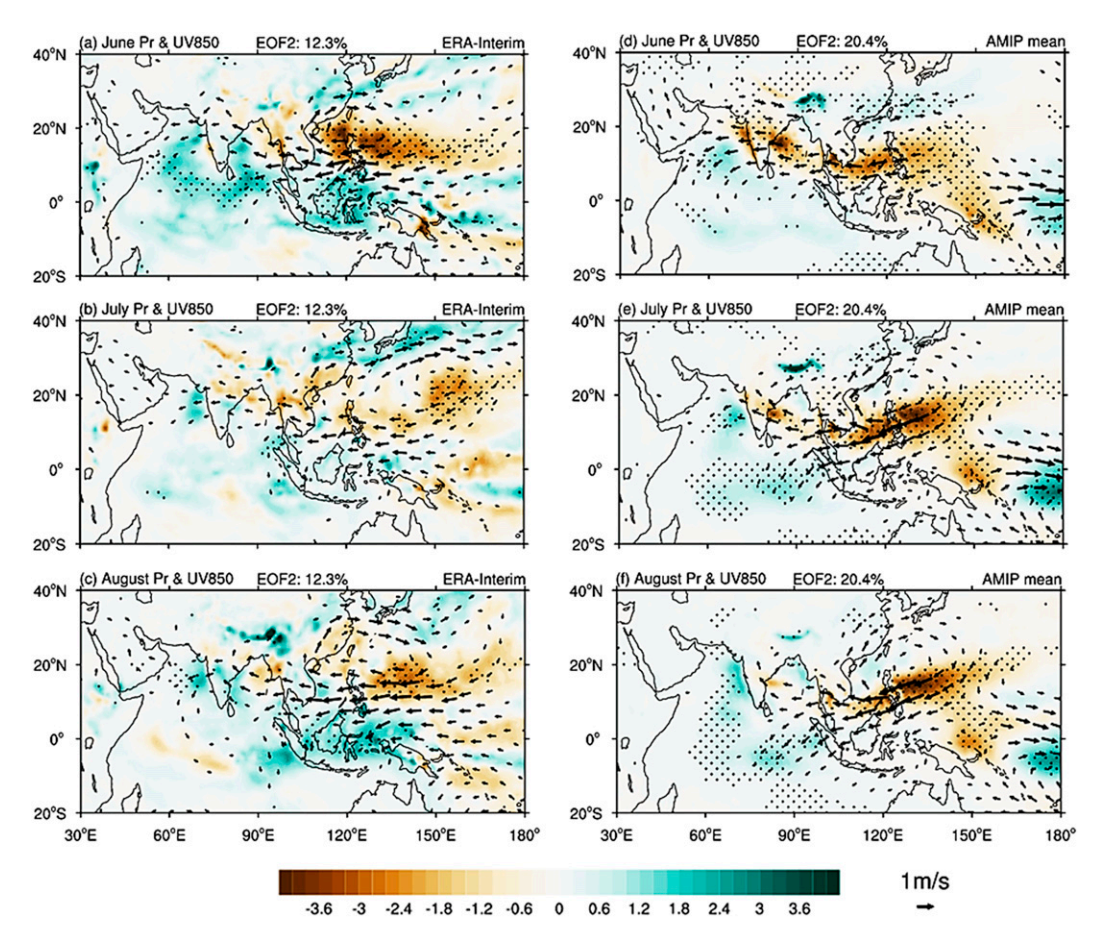


FIG. 3. As in Fig. 2, but for the month-reliant EOF PC₂^{SST}.

only the first two EOF modes are related to the underlying SST in observations. The negative Indian Ocean dipole (IOD)-like (Saji et al. 1999) wind anomalies in EOF₃^{SST} in observations, compared to the ensemble mean, are possibly due to the artifact of the month-reliant EOF method and may involve local air–sea interaction, which is unrelated to the ENSO forcing (Yang et al. 2015).

According to the month-reliant EOF analyses, an AAC over the NWP should persist during 2016 summer that follows a major El Niño event. However, the weak IPOC mode disappeared in August. Thus, the anomalous cyclone in August 2016 (Fig. 1c) over the NWP might be induced by the atmospheric internal variability.

b. Atmospheric internal mode

To extract the internal variability in August, we first use a linear regression model:

$$A = a_1^{\text{SST}} \times PC_1^{\text{SST}} + a_2^{\text{SST}} \times PC_2^{\text{SST}} + A^{\text{int}}, \qquad (1)$$

where A is the observational August mean upper and lower tropospheric wind anomalies, PC_1^{SST} and PC_2^{SST} are

the first two month-reliant EOF time series in observations, $a_1^{\rm SST}$ and $a_2^{\rm SST}$ denote the regression coefficients against the PC₁^{SST} and PC₂^{SST}, and the residual $A^{\rm int}$ is considered atmospheric internal variability. Then, we conduct an EOF analysis of normalized residual A int in the Indo-western Pacific region. Figure 6a shows rainfall and low-level wind anomalies regressed onto the first internal EOF PC (PC1int) in August. The dominant atmospheric internal mode in August shows a meridional rainfall dipole in the western Pacific with decreased precipitation centered on the south flank of the anomalous anticyclone in the NWP and increased rainfall over the Maritime Continent. The first mode accounts for 19.8% of total monthly wind variance and is well separated from the second mode. This internal mode (EOF₁^{int}) does not significantly correlate with the concurrent or antecedent Niño-3.4 index (-0.01 and 0.14, respectively). Aside from the opposite sign of rainfall and wind anomalies between Figs. 5c and 6a, the spatial pattern of EOF_3^{SST} resembles the EOF_1^{int} in August. Since the atmospheric internal variability is random in phase, we further check the atmospheric monthly

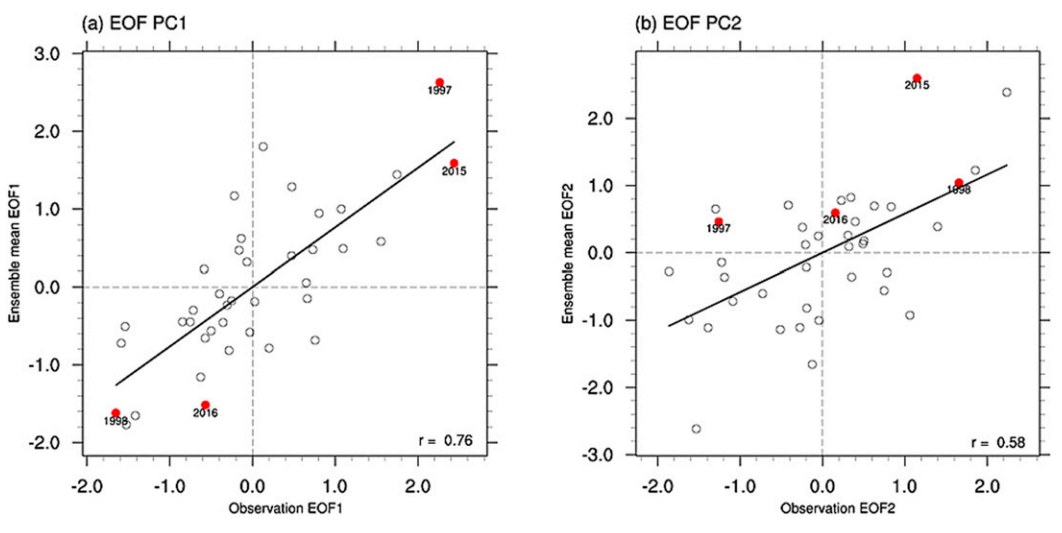


FIG. 4. Scatterplot between the month-reliant EOF PCs in observations and in the AMIP ensemble mean, for (a) PC_2^{SST} and (b) PC_2^{SST} . Black lines are the linear regressions. Red dots show two major El Niño developing summers (1997 and 2015) and post–El Niño summers (1998 and 2016).

evolution related to the August EOF_1^{int} by regressing the monthly rainfall and wind anomalies from June to August onto the August internal PC_1^{int} . The spatial pattern resembles the PC_3^{SST} of observations (not shown),

indicative of atmospheric internal variability of little temporal persistence. Interestingly, the August internal mode also resembles the IPOC mode with the pattern correlation of 850-hPa zonal wind anomalies amounting

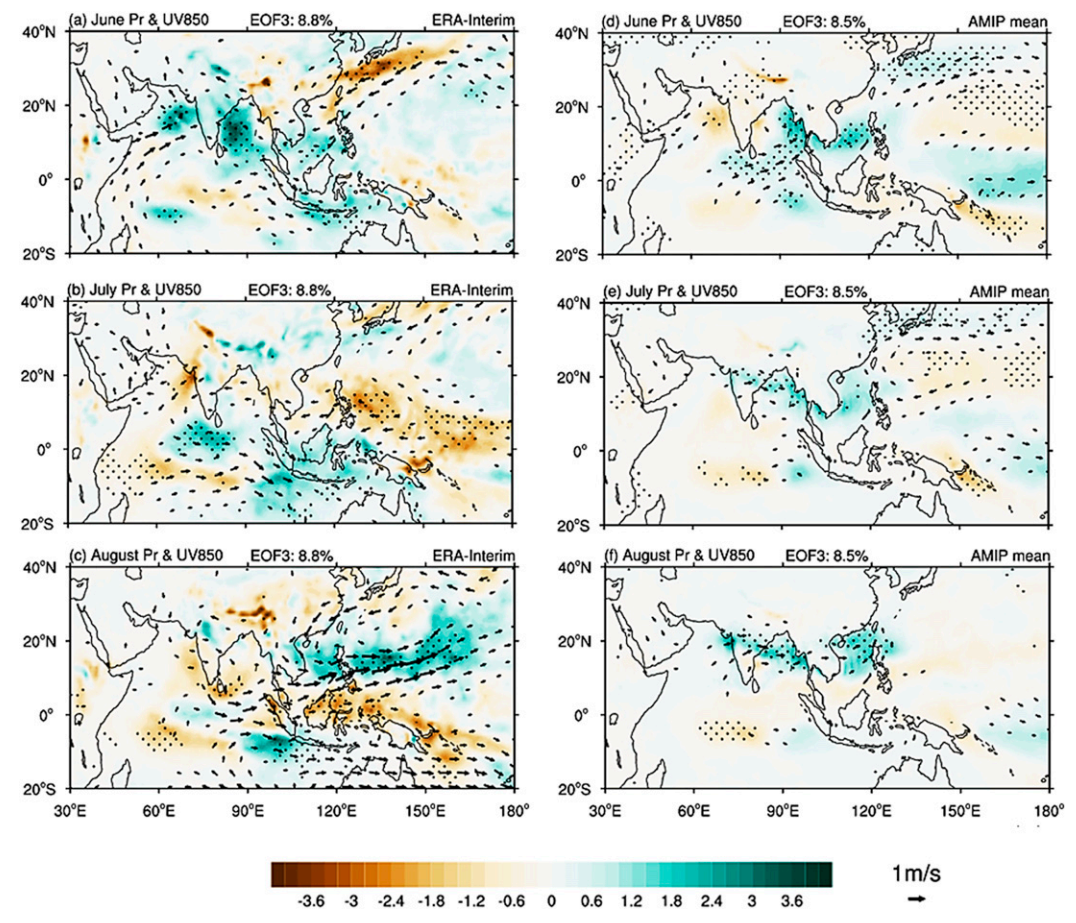


Fig. 5. As in Fig. 2, but for the month-reliant EOF PC_3^{SST} .

(b) August Pr & UV850

FOF1: 18%

Ensemble spread

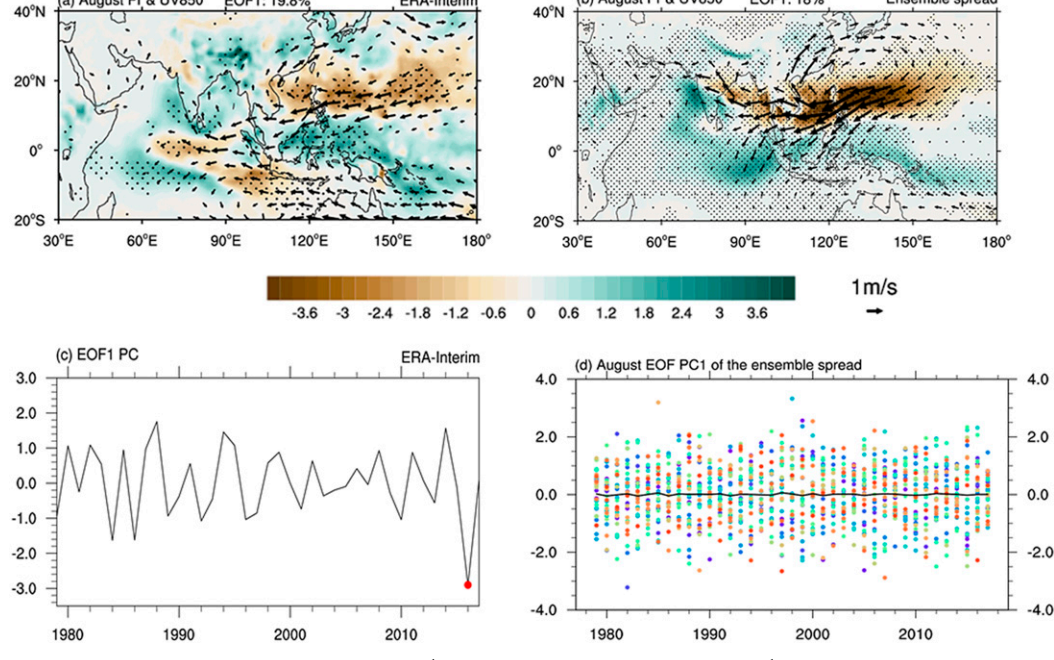


FIG. 6. August rainfall (shading; mm day $^{-1}$) and low-level wind (vectors; ms $^{-1}$) anomalies regressed against (a) the monthly internal EOF PC_1^{int} in observations and (b) the first EOF PC_1^{spd} of model ensemble spread. Stippling represents the rainfall anomalies >99% confidence level, based on the t test. (c) The time series of the principal component associated with the monthly internal EOF1, with year 2016 marked. (d) The principal component of the ensemble spread EOF1 in each member. Different color dots represent each member run, and the black curve shows the 30-member mean.

to 0.51. Although the NWP AAC is coupled with the external SST forcing (e.g., Indian Ocean warming) and regional air–sea interactions (Xie et al. 2009, 2016; Wang et al. 2018), it is also sustained through the kinetic energy conversions from the lower-level mean flow (Kosaka and Nakamura 2010; Huangfu et al. 2018; Hu et al. 2019).

In the AMIP model, the internal variability is simply the ensemble spread. Here we use the EOF method based on tandem 30-member ensemble spread to represent the atmospheric internal mode in August. Figure 6b shows the rainfall and 850-hPa wind anomalies regressed against the ensemble spread EOF PC1 (PC_1^{spd}). The first EOF mode (EOF₁^{spd}) of ensemble spread captures 18% of total wind variance and is separated from the second mode. The atmospheric internal mode in the intermember spread is almost identical to the internal mode EOF₁^{int} in observations. Compared to the observed EOF₁^{int}, the model result shows the "southwest-northeast" tilted wind pattern, consistent with the westward shift of tropical rainfall anomalies. The IOD-like low-level easterly wind anomalies over the eastern Indian Ocean in EOF₁^{int} cannot be found in the ensemble spread, indicating that the IOD is not part of atmospheric internal mode in observations. The phase of PC₁^{spd} is random and the ensemblemean PC_1^{spd} in each year is nearly zero (Fig. 6d). The model results confirm the robustness of the internal mode in observations as extracted with the EOF method. Figure 6c shows the PC time series of the August internal EOF₁^{int} in observations. The value of internal PC_1^{int} amounts to -2.9 in 2016, the largest in magnitude over the 39-yr record. This suggests that the internal variability plays an important role over the NWP in August 2016.

5. Internal mode due to the summer ISO

In sections 3 and 4, we compared the structure of the August internal mode between observations and the model ensemble spread. The results suggest that the unusual cyclone over the NWP in August 2016 is mainly due to the atmospheric internal variability. Shao et al. (2018) recently suggested the anomalous cyclone in August 2016 is related to the summer intraseasonal oscillation. The evolution of 7-day mean precipitation and 850-hPa wind anomalies from 6 July to 30 August 2016 (Fig. 7) supports that the enhanced convection propagates into the NWP in early August. The anomalous cyclone persists over the NWP from early August to 23 August and then advances northward rapidly. Here we

7-day Pre and UV850 Anomalies: 2016

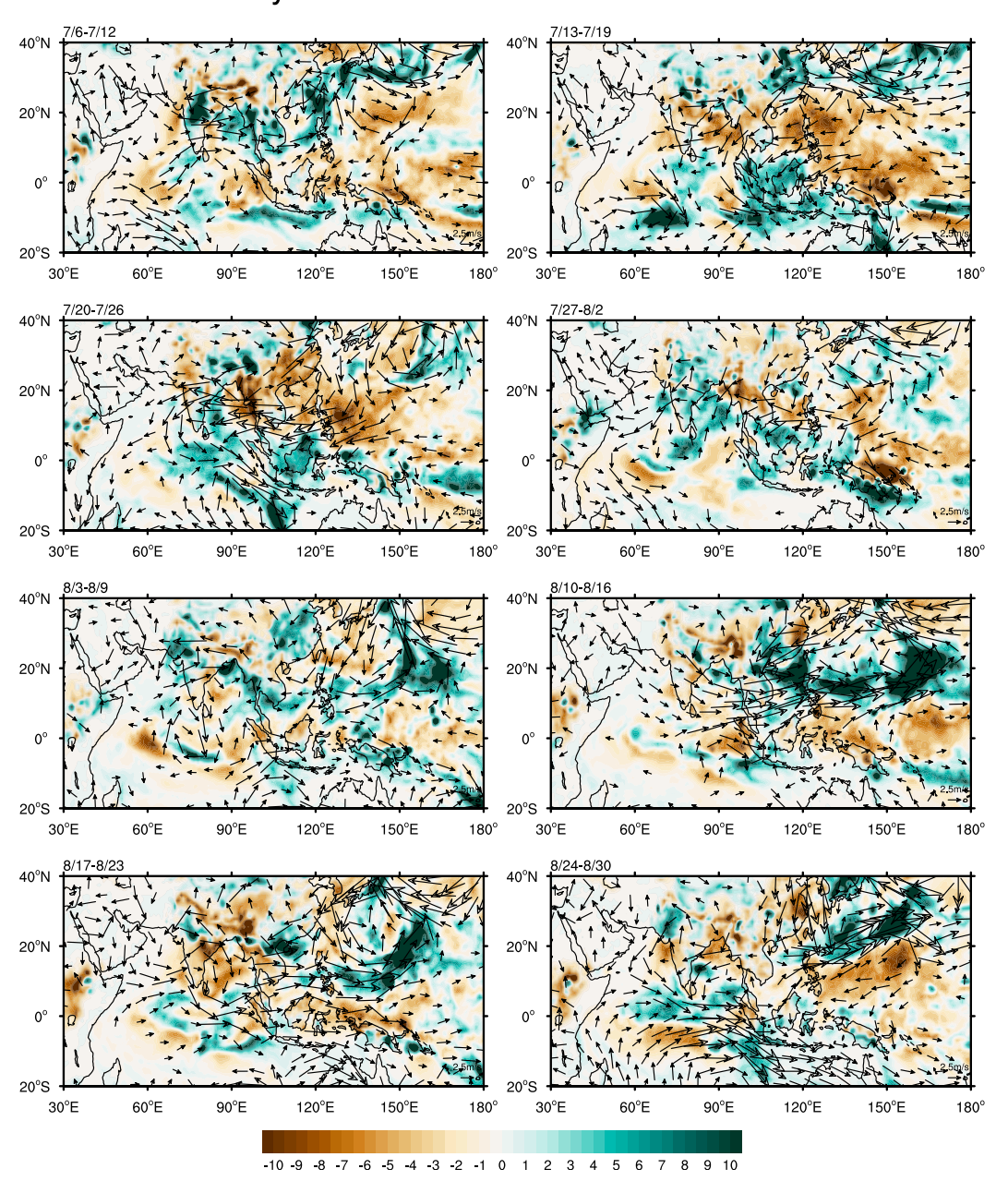


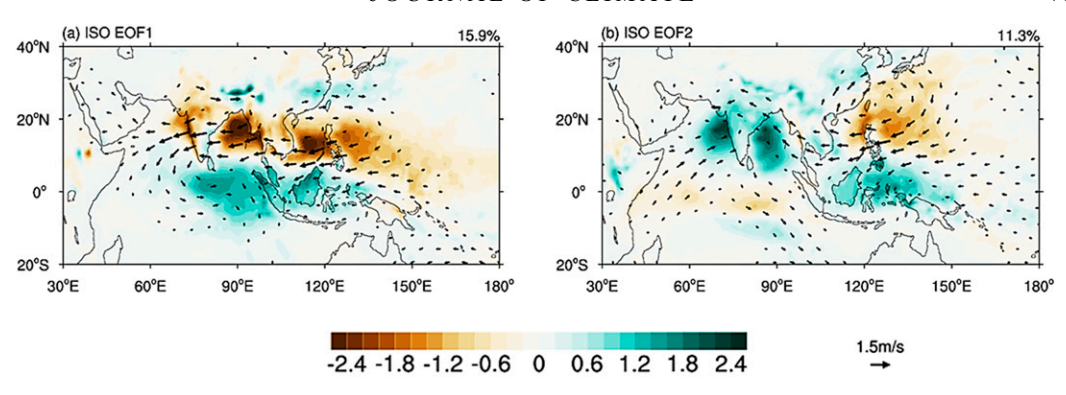
Fig. 7. Seven-day mean precipitation (shading; mm day $^{-1}$) and 850-hPa wind (vectors; m s $^{-1}$) anomalies from 6 Jul to 30 Aug 2016.

examine the relationship between the monthly internal mode and summer ISO over 39 years of 1979–2017.

a. Summer ISO

Figures 8a and 8b show the precipitation anomalies and 850-hPa winds regressed onto the first two EOF PCs of summer ISO (PC₁^{iso} and PC₂^{iso}). The first ISO mode (EOF₁^{iso}) captures 15.9% of total wind variance during the summer with zonally elongated rainfall anomalies.

The increased rainfall anomalies are located in the equatorial eastern Indian Ocean and the Maritime Continent, accompanied with negative anomalies from the Bay of Bengal, South China Sea, and their vicinity (Fig. 8a). Low-level wind anomalies show an anomalous anticyclonic circulation over the South China Sea to the NWP region. The easterly wind anomalies related to the anomalous anticyclone are northeasterly in the western Indian Ocean, causing the break of the summer



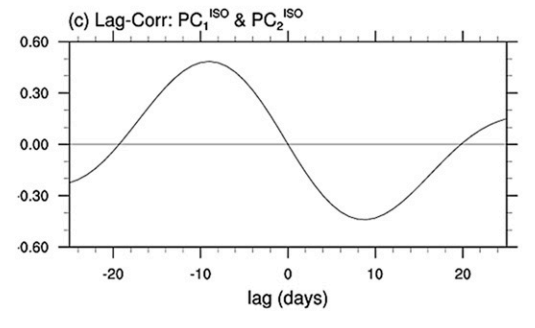


FIG. 8. (a),(b) Spatial structure of daily rainfall (shading) and 850-hPa wind (vectors) anomalies regressed onto the first two normalized ISO EOF PCs. (c) The lag correlations between the $PC_1^{\rm iso}$ and $PC_2^{\rm iso}$.

southwest monsoon (Goswami and Mohan 2001; Annamalai and Slingo 2001). The second EOF mode (EOF₂^{iso}) accounts for 11.3% of total wind variance (Fig. 8b), with a northwest-southeast-tilted rainband from the west coast of India to the Maritime Continent, accompanied with decreased precipitation anomalies over the NWP region. The EOF₂ features an AAC in the NWP of a broader meridional structure that is zonally displaced compared to the AAC in EOF₁iso. The strengthened southwesterlies in the northwestern Indian Ocean indicate the active phase of the Indian summer monsoon (Annamalai and Slingo 2001). Indeed, PC₁iso and PC_2^{iso} are correlated at 0.49 at 9-day lead (Fig. 8c). PC_1^{iso} and PC_2^{iso} show greatest coherence at the 30–40day range with a 90° phase difference (not shown). The strong coherence between PC1so and PC2so provides justification for combining them for a summer ISO index. Note that EOF3 and EOF4 represent the higherfrequency variations with the greatest coherence in the 10- to 20-day range and at the 30-day scale. EOFs 3 and 4 account for 12.9% of total variance and have small contributions to the monthly variability (not shown).

Figure 9 shows the composite of the precipitation and circulation fields for each of the eight phases. Following Wheeler and Hendon (2004), a life cycle of summer ISO is broken down into eight distinct phases. For the composite, each ISO phase has an amplitude $[(PC_1^{iso})^2 + (PC_2^{iso})^2]$ greater than 1. If the ISO has an amplitude smaller than 1, it is considered inactive. Positive rainfall anomalies associated with PC_1^{iso} first

appear over the equatorial eastern Indian Ocean in phase 1, and then propagate northward reaching India from phases 2 to 6 and the Bay of Bengal in phases 3–6. The convection over the equatorial eastern Indian Ocean also propagates eastward from phase 1 and reaches the Maritime Continent in phases 2–3. Then, the convection propagates northward reaching the South China Sea in phases 4–5, the NWP in phases 6–7 and East Asia with reduced amplitude in phase 8. Note that phase 7 features a meridional rainfall dipole between the Maritime Continent and the NWP region. The spatial pattern of ISO phase 7 is similar to the August monthly internal mode (Fig. 6a). This suggests the common spatial features between the monthly internal mode and summer ISO.

b. Mechanism for monthly internal mode

Now we examine the relationship between the August internal mode and the summer ISO. The August internal mode features the largest rainfall and wind variations over the NWP region, with much smaller loading over the Indian Ocean (Fig. 6). In contrast, summer ISO shows large rainfall and wind variations in the Indian Ocean (Fig. 9). Here we average ISO anomalies over August to explore the ISO relationship to the August internal mode. That is,

$$A^{\rm rec} = \sum_{1 \text{Aug}}^{31 \text{Aug}} \frac{(\text{EOF}_1^{\text{iso}} \text{PC}_1^{\text{iso}} + \text{EOF}_2^{\text{iso}} \text{PC}_2^{\text{iso}})}{31}, \quad (2)$$

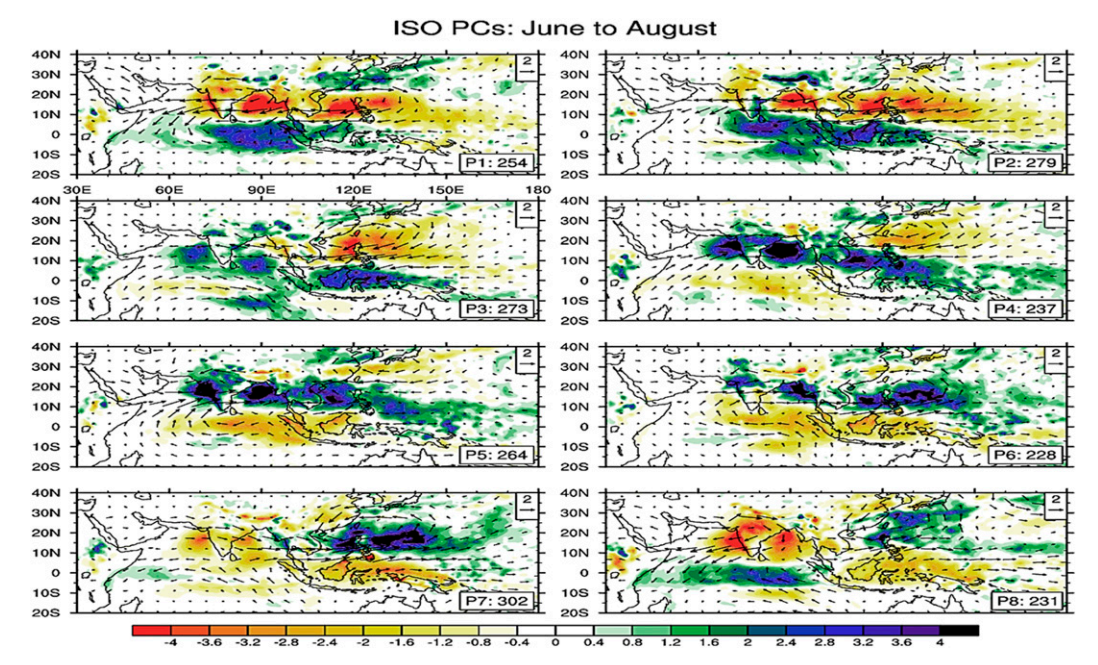


FIG. 9. The life cycle composite of rainfall (shading) and 850-hPa wind (vectors) anomalies reconstructed based on PC_2^{iso} and PC_2^{iso} of ISO in 8 phases. The number shown in the bottom right corner is the total days in each phase.

where A^{rec} is the August mean of reconstructed ISO wind anomalies based on the ISO modes 1 and 2. Figure 10 shows the first two EOF modes (EOF₁^{rec} and EOF₂^{rec}). EOF₁^{rec} explains 57.4% of total variance for the August mean of ISO variability. The spatial pattern is strikingly similar between the ISO reconstructed monthly mean EOF₁^{rec} (Fig. 10a) and the August internal mode EOF₁^{int} (Fig. 6a). The pattern correlation between EOF_1^{rec} and EOF_1^{int} in 40°-140°E, 10°S-25°N are 0.8 for low-level zonal wind and 0.78 for precipitation. The temporal correlation between the PC₁^{rec} and PC₁^{int} amounts to 0.65 (above the 99% significance level by using the t test). Compared to EOF $_1^{int}$, the spatial pattern of EOF₁^{rec} shows weak low-level wind anomalies in the Indian Ocean, suggesting limited contributions of IOD to the internal AAC over the NWP. The EOF₂^{rec} explains 42.6% of total variance and shows a slight weakening of all Indian summer monsoons (Fig. 10b). PC₂^{rec} is somewhat correlated with PC₂^{int} (not shown) with the correlation coefficient of 0.45, suggesting associations of ISO with the Indian summer monsoon internal variability (Goswami and Mohan 2001; Goswami and Xavier 2005; Zhou et al. 2019). The common spatial pattern between EOF₁^{rec} and EOF₁^{int} suggests that the ISO is an important contributor to the monthly internal mode. However, the convection center of the monthly-mean internal mode is mainly located in the NWP and resembles phase 7 of ISO rather than ISO EOF modes (phases 1 and 3 in Fig. 9).

The change in spatial pattern from ISO to the monthly internal mode might be due to the broadband nature of the ISO spectra (Fig. 11). The spectrum of PC_1^{iso} shows a peak at 60–90 days and secondary peak at 30–40 days while PC_2^{iso} has a strongest peak at 50–60 days and secondary peak at 30–40 days. Although the largest coherence between PC_1^{iso} and PC_2^{iso} is at 35–40 days, the ISO of a broader (30–90 days) band contributes to the monthly variability. We separate the intraseasonal variability into three bands (20–30, 30–40, and 40–90 days), and the results show that high-frequency (20–30 day) ISO contributes little to the monthly mean variations (not shown).

Figure 12 shows the fractional variance of August internal zonal wind explained by PC₁^{rec}. The EOF₁^{rec} accounts for more than 40% of monthly internal variance over the South China Sea and the NWP region. In summer, there is low-level confluence between the monsoonal westerlies and easterly trade winds over the NWP. The wave-mean flow interaction can amplify the monthly perturbations through the barotropic energy conversions, which is proportional to $[-(\partial \overline{u}/\partial x)(u'^2/2)]$ (Kosaka and Nakamura 2006, 2010). Hu et al. (2019) showed that the replenishing time scale of monthly anomalies by the barotropic energy conversion is about 5 days, fast enough to excite the intraseasonal to monthly perturbations within the low-level confluence zone. In addition, Huangfu et al. (2018) found that monthly anomalies over the NWP in August 2016 were associated with an eastward extension of the monsoon trough, with

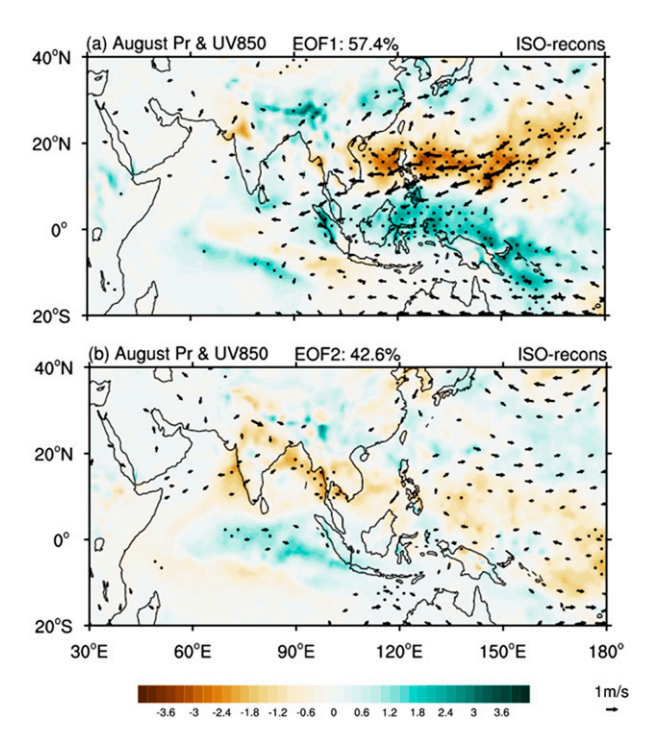


FIG. 10. August rainfall (shading) and 850-hPa wind (vectors) anomalies regressed onto the normalized ISO-reconstructed EOF: (a) PC_1^{rec} and (b) PC_2^{rec} . Stippling represents the rainfall anomalies >99% confidence level, based on the *t* test.

the barotropic energy conversions through the meridional shear of the mean zonal wind, $u'v'(\partial \overline{u}/\partial y)$. The diabatic heating in cumulus convection further amplifies the anomalies (Kosaka and Nakamura 2010). These studies suggest that the AAC grows on the barotropic conversion and convective feedback. In support of this notion, the reconstructed EOF₁^{rec} that represents the AAC explains large fractional variance only in the mean confluence zone (Fig. 12) even though ISO variance in zonal wind is high also over the north Indian Ocean (Fig. 8a).

6. Reconstructing the anomalies of summer 2016

We use the following regression model to reproduce the monthly anomalies for each summer month of 2016:

$$A' = a_1^{\text{SST}} \times \text{PC}_1^{\text{SST}} + a_2^{\text{SST}} \times \text{PC}_2^{\text{SST}} + \sum_{1 \le i \le N} \frac{(b_1^{\text{iso}} \times \text{PC}_1^{\text{iso}} + b_2^{\text{iso}} \times \text{PC}_2^{\text{iso}})}{M},$$
(3)

where A' is the monthly mean anomaly due to the SST forcing (the first two terms on the right-hand side) and ISO (last term of the right-hand side), and M is the number of days of the month. Table 1 shows the pattern correlation coefficients of reconstructed anomalies A'

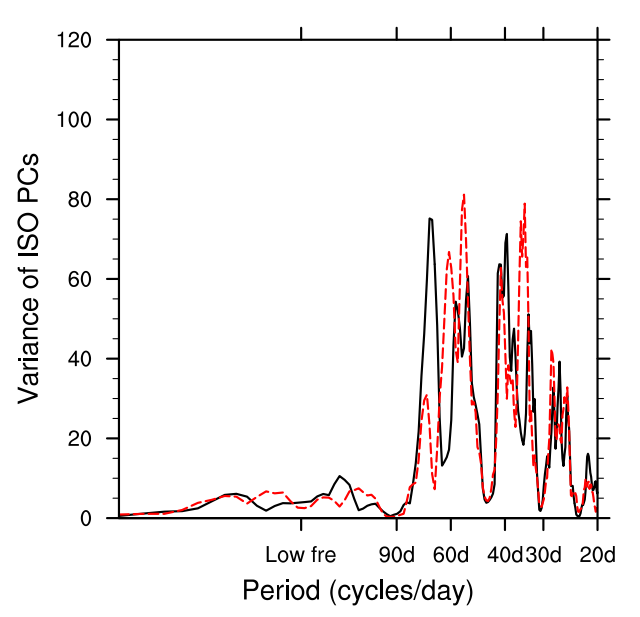


Fig. 11. Power spectra of the PC_1^{iso} (black solid line) and PC_2^{iso} (red dashed line).

with the raw monthly anomalies in 2016 over the NWP AAC domain (5°–35°N, 100°–155°E). By adding the ISO monthly mean to the regression model, we can successfully reproduce the monthly anomalies in each month of 2016 summer with a pattern correlation of zonal wind amounting to 0.82 in August. We further reconstruct the monthly anomalies without the ISO contribution (shown in parentheses in Table 1). The SST forcing by itself fails to reproduce the August anomalies over the NWP with a negative pattern correlation. By contrast, ISO does not

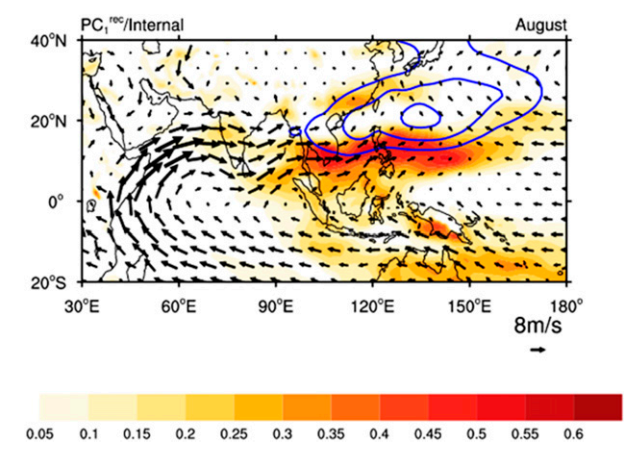


FIG. 12. Fraction of total variance of 850-hPa zonal wind explained by ISO-reconstructed monthly PC_1^{rec} . Black arrows show climatological wind (m s⁻¹) while blue contours denote the streamfunction anomalies (at intervals of 4 \times 10⁵ m s⁻¹ from 8 \times 10⁵ to 16 \times 10⁵ m s⁻¹) of EOF₁^{rec} at 850 hPa.

TABLE 1. Pattern correlations over 5°-35°N, 100°-155°E between the regression model reconstruction Eq. (3) and raw monthly anomalies for rainfall and low-level winds from June to August in 2016. For comparison, parentheses indicate the SST effect only.

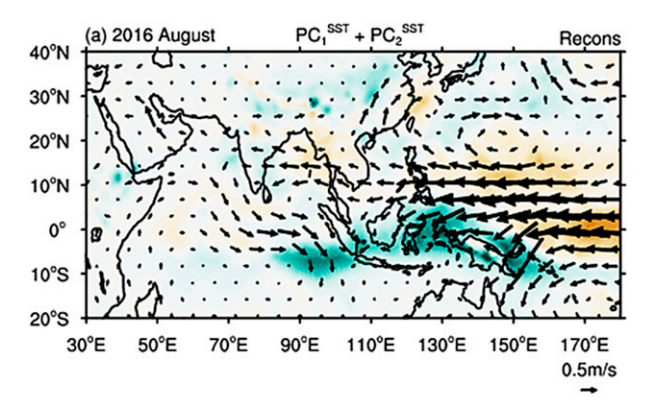
	Precipitation	U850	V850
June	0.31 (0.3)	0.54 (0.57)	0.29 (0.35)
July	0.58 (0.4)	0.71 (0.77)	0.4 (0.38)
August	0.63 (-0.06)	0.82(-0.47)	0.59 (-0.16)

contribute to the rainfall and wind anomalies in June and July in 2016. Figure 13 compares the reconstructed August anomalies over the Indo-NWP region with and without the ISO contribution. Without the ISO contribution, an anomalous anticyclone persists in August (Fig. 13a). By adding the ISO into the regression model, the low-level anomalous circulation turns cyclonic (Fig. 13b). The comparison shows that the anomalies of August 2016 are mainly due to the summer ISO.

7. Summary and discussion

We have investigated variability in monthly-mean atmospheric circulation over the Indo-western Pacific by using the EOF method in observations as well as an AMIP model ensemble. We show that the first two leading month-reliant EOF modes are related to the SST forcing, specifically concurrent and antecedent ENSO events. This is broadly consistent with the literature (Wang et al. 2003; Xie et al. 2009; Wang et al. 2018; Hu et al. 2019). The low-level circulation and rainfall patterns associated with slowly evolving oceanic forcing show strong spatial coherence and temporal persistence from June to August. Forced by observed SSTs, the AMIP ensemble mean well simulates Indo-western Pacific rainfall and circulation variations associated with ENSO.

We then examined the August-mean internal variability by subtracting the SST effects from the raw monthly anomalies. The leading internal mode in August resembles the IPOC mode with an AAC over the NWP albeit with little spatial coherence with either June or July anomalies. This suggests that the AAC can be forced by the ocean–atmosphere coupling (Xie et al. 2009, 2016) and may arise also from the atmospheric internal dynamics. During boreal summer, the low-level confluence exists between the monsoonal westerlies and easterly trade winds over the NWP, where perturbations gain kinetic energy from the mean flow through the barotropic energy conversions (Kosaka and Nakamura 2010; Hu et al. 2019). Thus, the mean zonal wind confluence helps anchor the AAC over the NWP. A similar internal mode





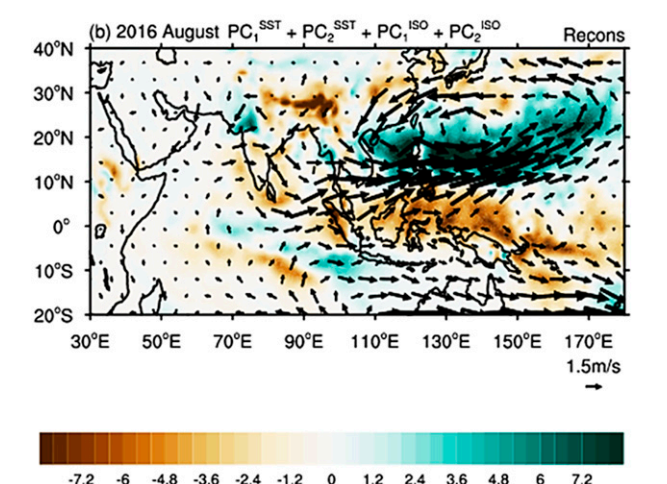


FIG. 13. Precipitation (shading; mm day⁻¹) and 850-hPa wind (vectors; m s⁻¹) anomalies in August 2016 reproduced by (a) the SST forcing (PC₁^{SST} + PC₂^{SST}) and (b) the SST forcing and the ISO contribution (PC₁^{SST} + PC₂^{SST} + PC₁^{iso} + PC₂^{iso}).

is found in other summer months, anchored in the mean confluence zone (not shown). The resemblance of the monthly internal mode with the IPOC indicates the structure of the mean flow is important for the NWP AAC formation. The lack of temporal persistence and spatial coherence in the internal mode from June to August is due to random phasing. The leading EOF mode for AMIP ensemble spread resembles the observed internal mode in further support of our observational analysis.

We identified a relationship between the monthly internal mode and the summer ISO. The first EOF mode of ISO-reconstructed monthly mean is very similar to the monthly internal mode, both with the AAC over the NWP. The broadband spectrum of the ISO contributes

to the monthly internal mode. About 50% of total monthly internal variance of low-level zonal wind over the NWP can be explained by the summer ISO (Fig. 12). While a similar relationship between the summer monsoon ISO and the interannual variability has been identified over a limited domain of the Indian Ocean (Goswami and Mohan 2001; Goswami and Xavier 2005), we showed that the ISO contribution to the internal variability is largest over the NWP. Our results indicate strong interactions across different time scales over the NWP.

Following the major El Niño of 2015/16, an AAC develops over the NWP in June–July 2016, consistent with the IPOC. The anomalous circulation switches to cyclonic in August 2016 over the NWP. The AMIP ensemble mean fails to reproduce the anomalies of August 2016, suggesting limited SST contributions. We show that the unusual circulation and rainfall anomalies in August 2016 arise from the summer ISO. In fact, the ISO-related internal mode sets the 39-yr record of 1979–2017 in magnitude in August 2016.

We separate SST-forced and atmospheric internal variability based on the linear regression. Goswami and Xavier (2005) suggest that nonlinear interactions between MISO and seasonal mean internal variability, with land surface processes playing a role. In addition, Li et al. (2017) found that the NWP climate anomalies in August 2016 are related to the Silk Road teleconnection, with wave energy propagation along the midlatitude westerly jet (Xu et al. 2019). Further studies are needed in these areas.

Acknowledgments. We wish to thank Mike Wallace (University of Washington) for useful discussions and suggestions. X. W. and Z. G. are supported by the Natural Science Foundation of China (41330425) and Jiangsu PAPD project, and S.-P. X. by the U.S. National Science Foundation (1637450). X.W. is also supported by the China Scholarship Council (201708320296). Plots are created with the NCAR Command Language (http://dx.doi.org/10.5065/D6WD3XH5).

REFERENCES

- Adames, Á. F., J. M. Wallace, and J. M. Monteiro, 2016: Seasonality of the structure and propagation characteristics of the MJO. J. Atmos. Sci., 73, 3511–3526, https://doi.org/ 10.1175/JAS-D-15-0232.1.
- Alexander, M. A., I. Bladé, M. Newman, J. R. Lanzante, N.-C. Lau, and J. D. Scott, 2002: The atmospheric bridge: The influence of ENSO teleconnections on air–sea interaction over the global oceans. *J. Climate*, **15**, 2205–2231, https://doi.org/10.1175/1520-0442(2002)015<2205:TABTIO>2.0.CO;2.
- Annamalai, H., and J. M. Slingo, 2001: Active/break cycles: Diagnosis of the intraseasonal variability of the Asian summer

- monsoon. Climate Dyn., **18**, 85–102, https://doi.org/10.1007/s003820100161.
- Chen, D., Y. Gao, and H. Wang, 2019: Why was the August rainfall pattern in the East Asia–Pacific Ocean region in 2016 different from that in 1998 under a similar preceding El Niño background? *J. Climate*, 32, 5785–5797, https://doi.org/10.1175/ JCLI-D-18-0589.1.
- Chowdary, J. S., G. Srinivas, Y. Du, K. Gopinath, C. Gnanaseelan, A. Parekh, and P. Singh, 2019: Month-to-month variability of Indian summer monsoon rainfall in 2016: Role of the Indo-Pacific climatic conditions. *Climate Dyn.*, 52, 1157–1171, https://doi.org/10.1007/s00382-018-4185-4.
- Dee, D. P., and Coauthors, 2011: The ERA-Interim reanalysis: Configuration and performance of the data assimilation system. *Quart. J. Roy. Meteor. Soc.*, **137**, 553–597, https://doi.org/10.1002/qj.828.
- Deser, C., M. A. Alexander, S. P. Xie, and A. S. Phillips, 2010: Sea surface temperature variability: Patterns and mechanisms. *Annu. Rev. Mar. Sci.*, 2, 115–143, https://doi.org/10.1146/ annurev-marine-120408-151453.
- Du, Y., S. P. Xie, G. Huang, and K. Hu, 2009: Role of air–sea interaction in the long persistence of El Niño–induced north Indian Ocean warming. *J. Climate*, 22, 2023–2038, https://doi.org/10.1175/2008JCLI2590.1.
- Duchon, C. E., 1979: Lanczos filtering in one and two dimensions. *J. Appl. Meteor.*, **18**, 1016–1022, https://doi.org/10.1175/1520-0450(1979)018<1016:LFIOAT>2.0.CO;2.
- Goswami, B. N., 1998: Interannual variations of Indian summer monsoon in a GCM: External conditions versus internal feedbacks. *J. Climate*, **11**, 501–522, https://doi.org/10.1175/1520-0442(1998)011<0501:IVOISM>2.0.CO;2.
- —, 2012: South Asian monsoon. *Intraseasonal Variability in the Atmosphere–Ocean Climate System*, W. K. M. Lau and D. E. Waliser, Eds., Springer, 21–72.
- —, and R. A. Mohan, 2001: Intraseasonal oscillations and interannual variability of the Indian summer monsoon. J. Climate, 14, 1180–1198, https://doi.org/10.1175/1520-0442(2001) 014<1180:IOAIVO>2.0.CO;2.
- ——, and P. K. Xavier, 2005: Dynamics of "internal" interannual variability of the Indian summer monsoon in a GCM. *J. Geophys. Res.*, 110, D24104, https://doi.org/10.1029/2005JD006042.
- Hsu, P.-C., J.-Y. Lee, K.-J. Ha, and C.-H. Tsou, 2017: Influences of boreal summer intraseasonal oscillation on heat waves in monsoon Asia. J. Climate, 30, 7191–7211, https://doi.org/ 10.1175/JCLI-D-16-0505.1.
- Hu, K., G. Huang, S. P. Xie, and S. M. Long, 2019: Effect of the mean flow on the anomalous anticyclone over the Indo-Northwest Pacific in post-El Niño summers. *Climate Dyn.*, 53, 5725–5741, https://doi.org/10.1007/S00382-019-04893-Z.
- Huangfu, J., R. Huang, W. Chen, and T. Feng, 2018: Causes of the active typhoon season in 2016 following a strong El Niño with a comparison to 1998. *Int. J. Climatol.*, 38, e1107–e1118, https://doi.org/10.1002/joc.5437.
- Hurrell, J. W., J. J. Hack, D. Shea, J. M. Caron, and J. Rosinski, 2008: A new sea surface temperature and sea ice boundary dataset for the Community Atmosphere Model. J. Climate, 21, 5145–5153, https://doi.org/10.1175/2008JCLI2292.1.
- Jiang, X., Á. F. Adames, M. Zhao, D. Waliser, and E. Maloney, 2018: A unified moisture mode framework for seasonality of the Madden–Julian oscillation. *J. Climate*, 31, 4215–4224, https://doi.org/10.1175/JCLI-D-17-0671.1.
- Joseph, P. V., J. K. Eischeid, and R. J. Pyle, 1994: Interannual variability of the onset of the Indian summer monsoon and its

- association with atmospheric features, El Niño, and sea surface temperature anomalies. *J. Climate*, **7**, 81–105, https://doi.org/10.1175/1520-0442(1994)007<0081: IVOTOO>2.0.CO:2.
- Kosaka, Y. and H. Nakamura, 2006: Structure and dynamics of the summertime Pacific–Japan teleconnection pattern. Quart. J. Roy. Meteor. Soc., 132, 2009–2030, https://doi.org/10.1256/qj.05.204.
- —, and —, 2010: Mechanisms of meridional teleconnection observed between a summer monsoon system and a subtropical anticyclone. Part I: The Pacific–Japan pattern. *J. Climate*, 23, 5085–5108, https://doi.org/10.1175/2010JCLI3413.1.
- —, S.-P. Xie, N.-C. Lau, and G. A. Vecchi, 2013: Origin of seasonal predictability for summer climate over the Northwestern Pacific. *Proc. Natl. Acad. Sci. USA*, **110**, 7574–7579, https://doi.org/10.1073/pnas.1215582110.
- Lee, J.-Y., B. Wang, M. C. Wheeler, X. Fu, D. E. Waliser, and I.-S. Kang, 2013: Real-time multivariate indices for the boreal summer intraseasonal oscillation over the Asian summer monsoon region. *Climate Dyn.*, 40, 493–509, https://doi.org/10.1007/s00382-012-1544-4.
- Li, C., W. Chen, X. Hong, and R. Lu, 2017: Why was the strengthening of rainfall in summer over the Yangtze River valley in 2016 less pronounced than that in 1998 under similar preceding El Nino events?—Role of midlatitude circulation in August. Adv. Atmos. Sci., 34, 1290–1300, https://doi.org/ 10.1007/s00376-017-7003-8.
- Madden, R. A., and P. R. Julian, 1971: Detection of a 40–50 day oscillation in the zonal wind in the tropical Pacific. *J. Atmos. Sci.*, 28, 702–708, https://doi.org/10.1175/1520-0469(1971) 028<0702:DOADOI>2.0.CO;2.
- —, and —, 1972: Description of global-scale circulation cells in the tropics with a 40–50 day period. *J. Atmos. Sci.*, 29, 1109–1123, https://doi.org/10.1175/1520-0469(1972)029<1109: DOGSCC>2.0.CO;2.
- Mao, J., and G. Wu, 2006: Intraseasonal variations of the Yangtze rainfall and its related atmospheric circulation features during the 1991 summer. *Climate Dyn.*, 27, 815–830, https://doi.org/ 10.1007/s00382-006-0164-2.
- Mishra, V., B. V. Smoliak, D. P. Lettenmaier, and J. M. Wallace, 2012: A prominent pattern of year-to-year variability in Indian summer monsoon rainfall. *Proc. Natl. Acad. Sci. USA*, **109**, 7213–7217, https://doi.org/10.1073/pnas.1119150109.
- Murakami, T., L. X. Chen, and A. Xie, 1986: Relationship among seasonal cycles, low-frequency oscillations, and transient disturbances as revealed from outgoing longwave radiation data. *Mon. Wea. Rev.*, 114, 1456–1465, https://doi.org/10.1175/1520-0493(1986)114<1456:RASCLF>2.0.CO;2.
- Nitta, T., 1987: Convective activities in the tropical western Pacific and their impact on the Northern Hemisphere summer circulation. J. Meteor. Soc. Japan, 65, 373–390, https://doi.org/ 10.2151/jmsj1965.65.3_373.
- North, G. R., T. L. Bell, R. F. Cahalan, and F. J. Moeng, 1982: Sampling errors in the estimation of empirical orthogonal functions. *Mon. Wea. Rev.*, **110**, 699–706, https://doi.org/10.1175/1520-0493(1982)110<0699:SEITEO>2.0.CO;2.
- Rasmusson, E. M., and T. H. Carpenter, 1983: The relationship between eastern equatorial Pacific sea surface temperatures and rainfall over India and Sri Lanka. *Mon. Wea. Rev.*, 111, 517–528, https://doi.org/10.1175/1520-0493(1983)111<0517: TRBEEP>2.0.CO;2.
- Rayner, N. A., D. E. Parker, E. B. Horton, C. K. Folland, L. V. Alexander, D. P. Rowell, E. C. Kent, and A. Kaplan, 2003: Global analyses of sea surface temperature, sea ice, and

- night marine air temperature since the late nineteenth century. *J. Geophys. Res.*, **108**, 4407, https://doi.org/10.1029/2002JD002670.
- Reynolds, R. W., N. A. Rayner, T. M. Smith, D. C. Stokes, and W. Wang, 2002: An improved in situ and satellite SST analysis for climate. *J. Climate*, **15**, 1609–1625, https://doi.org/10.1175/1520-0442(2002)015<1609:AIISAS>2.0.CO;2.
- Roeckner, E., Coauthors, 2003: The atmospheric general circulation model ECHAM 5. Part I: Model description. Max Planck Institute for Meteorology Rep. 349, 127 pp.
- Saji, N. H., B. N. Goswami, P. N. Vinayachandran, and T. Yamagata, 1999: A dipole mode in the tropical Indian Ocean. *Nature*, 401, 360–363, https://doi.org/10.1038/43854.
- Shao, X., S. Li, N. Liu, and J. Song, 2018: The Madden–Julian oscillation during the 2016 summer and its possible impact on rainfall in China. *Int. J. Climatol.*, 38, 2575–2589, https://doi.org/10.1002/joc.5440.
- Sperber, K. R., J. M. Slingo, and H. Annamalai, 2000: Predictability and the relationship between subseasonal and interannual variability during the Asian summer monsoon. *Quart. J. Roy. Meteor. Soc.*, **126**, 2545–2574, https://doi.org/10.1002/qj.49712656810.
- Takaya, Y., Y. Kubo, S. Maeda, and S. Hirahara, 2017: Prediction and attribution of quiescent tropical cyclone activity in the early summer of 2016: Case study of lingering effects by preceding strong El Niño events. *Atmos. Sci. Lett.*, 18, 330–335, https://doi.org/10.1002/asl.760.
- Trenberth, K. E., J. M. Caron, D. P. Stepaniak, and S. Worley, 2002: Evolution of El Niño–Southern Oscillation and global atmospheric surface temperatures. *J. Geophys. Res.*, **107**, 4065, https://doi.org/10.1029/2000JD000298.
- Wang, B., and H. Rui, 1990: Synoptic climatology of transient tropical intraseasonal convection anomalies: 1975–1985. *Meteor. Atmos. Phys.*, 44, 43–61, https://doi.org/10.1007/ BF01026810.
- —, R. Wu, and T. Li, 2003: Atmosphere–warm ocean interaction and its impacts on Asian–Australian monsoon variation. *J. Climate*, 16, 1195–1211, https://doi.org/10.1175/1520-0442(2003) 16<1195:AOIAII>2.0.CO;2.
- Wang, C.-Y., S.-P. Xie, and Y. Kosaka, 2018: Indo-western Pacific climate variability: ENSO forcing and internal dynamics in a tropical Pacific pacemaker simulation. *J. Climate*, 31, 10123– 10139, https://doi.org/10.1175/JCLI-D-18-0203.1.
- —, —, and —, 2020: ENSO-unrelated variability in Indo-Northwest Pacific climate: Regional and coupled oceanatmospheric feedback. J. Climate, https://doi.org/10.1175/ JCLI-D-19-0426.1, in press.
- Webster, P. J., and S. Yang, 1992: Monsoon and ENSO: Selectively interactive systems. *Quart. J. Roy. Meteor. Soc.*, 118, 877–926, https://doi.org/10.1002/qj.49711850705.
- —, V. O. Magaña, T. N. Palmer, J. Shukla, R. A. Tomas, M. U. Yanai, and T. Yasunari, 1998: Monsoons: Processes, predictability, and the prospects for prediction. *J. Geophys. Res.*, 103, 14 451–14 510, https://doi.org/10.1029/97JC02719.
- Wheeler, M. C., and H. H. Hendon, 2004: An all-season real-time multivariate MJO index: Development of an index for monitoring and prediction. *Mon. Wea. Rev.*, 132, 1917–1932, https:// doi.org/10.1175/1520-0493(2004)132<1917:AARMMI>2.0.CO;2.
- Wu, B., T. Li, and T. Zhou, 2010: Relative contributions of the Indian Ocean and local SST anomalies to the maintenance of the western North Pacific anomalous anticyclone during the El Niño decaying summer. *J. Climate*, 23, 2974–2986, https:// doi.org/10.1175/2010JCLI3300.1.

- Xie, S.-P., K. Hu, J. Hafner, H. Tokinaga, Y. Du, G. Huang, and T. Sampe, 2009: Indian Ocean capacitor effect on Indo-western Pacific climate during the summer following El Niño. J. Climate, 22, 730–747, https://doi.org/10.1175/2008JCLI2544.1.
- —, Y. Kosaka, Y. Du, K. Hu, J. S. Chowdary, and G. Huang, 2016: Indo-western Pacific Ocean capacitor and coherent climate anomalies in post-ENSO summer: A review. *Adv. Atmos. Sci.*, **33**, 411–432, https://doi.org/10.1007/s00376-015-5192-6.
- Xu, P., L. Wang, W. Chen, J. Feng, and Y. Liu, 2019: Structural changes in the Pacific–Japan pattern in the late 1990s. J. Climate, 32, 607–621, https://doi.org/10.1175/JCLI-D-18-0123.1.
- Yang, Y., S.-P. Xie, L. Wu, Y. Kosaka, N.-C. Lau, and G. A. Vecchi, 2015: Seasonality and predictability of the Indian Ocean dipole mode: ENSO forcing and internal variability. *J. Climate*, 28, 8021–8036, https://doi.org/10.1175/JCLI-D-15-0078.1.

- Yasunari, T., 1980: A quasi-stationary appearance of 30 to 40 day period in the cloudiness fluctuations during the summer monsoon over India. *J. Meteor. Soc. Japan*, **58**, 225–229, https://doi.org/10.2151/jmsj1965.58.3_225.
- Zhang, C., 2005: Madden-Julian oscillation. Rev. Geophys., 43, RG2003, https://doi.org/10.1029/2004RG000158.
- Zhang, R., A. Sumi, and M. Kimoto, 1999: A diagnostic study of the impact of El Niño on the precipitation in China. *Adv. Atmos. Sci.*, **16**, 229–241, https://doi.org/10.1007/BF02973084.
- Zhou, Z.-Q., S.-P. Xie, G. J. Zhang, and W. Zhou, 2018: Evaluating AMIP skill in simulating interannual variability over the Indowestern Pacific. *J. Climate*, **31**, 2253–2265, https://doi.org/10.1175/JCLI-D-17-0123.1.
- —, R. Zhang, and S. P. Xie, 2019: Interannual variability of summer surface air temperature over central India: Implications for monsoon onset. *J. Climate*, 32, 1693–1706, https://doi.org/ 10.1175/JCLI-D-18-0675.1.